24th EUROPEAN ROTORCRAFT FORUM
Marseille, France - 15th-17th September 1998

REFERENCE : AE11

TITLE : Computation of Helicopter Rotor Wake Using a High Order Panel Method

G. COPPENS, M. COSTES
ONERA, Châtillon, France

A. LEROY, P. DEVINANT
LME, ESEM, University of Orléans, France

The paper describes a new development brought to the MESIR free-wake model currently used at ONERA and EUROCOPTER. This new time-marching method, called MINT, is based on the mathematical theory of vortex sheets in three-dimensional unsteady flows established by Mudry. The vortex sheet is represented by a couple ($\vec{\varpi}$, $\bar{\gamma}$) which gives a complete description of its evolution. A higher order space discretisation is used, where the wake is represented by panels on which the circulation varies linearly. Induced velocities are computed by a Gauss integration technique, and no regularisation is applied. Applications to the BO 105 rotor in descent flight conditions show the good stability and convergence of the method which is also more efficient than MESIR in terms of computer cost.

INTRODUCTION

Helicopter differs from other aircraft by its rotary wing which ensures both the lift and the propulsion of the rotorcraft. Indeed, the main lifting surface of the helicopter has a combination of translation and rotation motions which render the flowfield around the rotor extremely complex because of the various aerodynamic phenomena encountered during the blade rotation. One can mention three-dimensionality, unsteadiness, non-linear transonic conditions, large viscous and rotational effects on the flowfield.

The unsteadiness in forward flight is first introduced by the freestream velocity varying with azimuth, and consequently by the complex dynamic motion which is thus necessary to trim the rotor. In manoeuvre, the time-varying helicopter speed adds to the flowfield unsteadiness. At high-speed forward flight, transonic conditions are present at the blades tip where compressible flow and shock waves appear.

Otherwise, rotational effects are particularly important in hover or descent flight, when the wake shed from the blades remains very close to the rotor disk, thus creating interactions and noise. This blade vortex interaction phenomenon (BVI) has become an increasingly important problem for helicopter designers [1]. Indeed, BVI causes sudden changes in blade loading which contribute to the characteristic blade « slap » emitted by the helicopter and which can be heard during approach and landing. This impulsive noise is especially penalising for the use of helicopter in civil applications, particularly in a urban environment, and allows the detectability of military helicopters as well.

Moreover, the wake can interact with the fuselage in certain types of motion. This is especially true during transition between hover and forward flight, when the main rotor wake is convected towards the tail surfaces, creating thus rotorcraft control perturbations (e.g. pitch up). Hence, structural and vibration problems also happen on the fuselage, as well as helicopter control difficulties may be created by this wake passage.

All these features make the computation of the complete flowfield around a helicopter very difficult and not feasible with current computer capabilities. This is why most of the methods try to address one of these features only.

As noted above, the rotor wake is a major phenomenon in almost all helicopter problems, therefore it is important for designers to have efficient aerodynamic computations applied to helicopters to predict these interactions and thus improve new designs.

Different numerical techniques can be used to predict the rotor wake characteristics.

The Navier-Stokes methods describe both the viscous and rotational phenomena which constitute the wake. However the grid fineness needed to obtain accurate results cannot be reached with present computer capabilities, and this model

is still not practicable for a full 3D wake computation without excessive numerical diffusion [2][3]. The Euler equations are an inviscid approximation of the Navier-Stokes equations, which capture and convect the vorticity in the flowfield. Numerical solutions to the Euler equations have the same drawbacks as those of the Navier-Stokes, namely the diffusion of the wake [4][5]. Different approaches have been developed to solve this diffusion problem. One of them is the Eulerian-Lagrangian coupling [6][7] which decouples the wake description into two sets of equations, the Eulerian approach being able to capture the vortex sheets and the Lagrangian approach to convect them with limited diffusion. Another promising approach is the vorticity confinement of Steinhoff [8] which reconcentrates the vorticity into the wake sheets.

The Full Potential equation does not capture the rotational effects and deals with vortex sheets as potential discontinuities. The wake geometry is therefore depending on the geometry of the grid. However, a coupled Eulerian-Lagragian methodology has also been developed for the Full Potential equation [9][10] using markers which are freely convected in the computational grid. These markers carry a normal velocity component equivalent to a potential discontinuity across the wake sheet, and this velocity is distributed to the neighbouring grid cells, allowing thus to account for the actual wake geometry in the computation. Nevertheless, although this approach allows to account for the free-wake geometry in the compressible flowfield without numerical diffusion, the methodology is heavy and difficult to implement.

Indeed, the compressibility has little effect on helicopter rotor wakes due to their low convection speed, and this explains the popularity of panel methods to compute them [11][12][13][14][15][16].

Ahmed [17] uses an unsteady panel method to do so. Wake and blades are divided into finite surface elements carrying a source/sink plus a doublet distribution. Hence, using the Stokes-Ampere equations, doublet panels are replaced by vortex rings. The doublet distribution is thus supposed to be constant on each panel. This method allows a step by step resolution of the wake, but it does not account for the compressibility effect which cannot be neglected on the blade itself.

This is why a number of vortex-lattice free wake codes (e.g. MESIR [18]) simulate blades by lifting lines, which allow to use experimental airfoil data to estimate the blade loads. The velocities induced by the wake are computed for all points on the rotor disk and their wake nodes using the Biot-Savart law and are added to the rotor motion to convect the wake. This methodology gives an accurate prediction of blades loading at a reasonable cost. However, most of these methods consider the flowfield to be periodic in time, so that true unsteady conditions such as those encountered during manoeuvre flight cannot be considered. Another restriction of a large number of these methods is that they consider the tip vortex only and therefore cannot account for complex rolling-up phenomena which can be obtained in the inner sheet.

This paper presents a new time-marching approach which is being developed at ONERA to compute the free-wake evolution of a helicopter rotor undergoing any type of motion (in particular manoeuvre). This method, called MINT, is being built on the basis of the MESIR free-wake code which is capable to deal with steady forward flight conditions only, and uses a general mathematical description of vortex sheets for an incompressible flow. In a first part of the paper, an outline of this theory is given. Then, its numerical implementation is described, with an emphasis on specific problems to helicopter. A first validation of the method is then presented with a restriction to steady level and descent flight conditions because of the quasi-steady assumption made to compute the blade loads at the present status of the method. Future evolutions of this methodology are finally described.

DESCRIPTION OF THE METHOD

In order to accurately predict the complex flow associated with the rotor wake, the general theory of vortex sheets in unsteady flow developed by Mudry [19] has been applied.

This theory gives a rigorous mathematical description of the incompressible vortex sheet evolution and the main results are summarised here. In the case of a viscous fluid, the flow is irrotationnal over the entire flowfield, except at the body's solid boundaries and in the wake. The two boundary layers from the upper (+) and the lower (-) surfaces generate the wake downstream the body (fig. 1). In the case of evanescent viscosity, the wake has to be considered as an infinitely thin layer, which is the union of two sheets S^+ and S^- tangent with the body surface on the upper and the lower points of separation on the body respectively and in contact with each other downstream it. This is why for an inviscid fluid, the wake Σ is a slip surface :

$$\vec{U}^+ . \vec{n} = \vec{U}^- . \vec{n} \text{ on } \Sigma. \qquad (1)$$

Assuming the following assumptions : inviscid, irrotational, incompressible fluid, a velocity

potential Φ can be determined subject to the following conditions :

- Φ verifies the Laplace equation :

$$\nabla^2\Phi(x,t)=0. \qquad (2)$$

- the fluid is undisturbed far away from the blades and the wake

$$\Phi\to 0 \text{ as } |r-r_{blades}|\to\infty \qquad (3)$$
$$\Phi\to 0 \text{ as } |r-r_{wake}|\to\infty$$

- Φ satisfies the Kutta-Joukowski condition at the trailing edge of the body.

In the following description, blades are represented by Prandtl's lifting-lines, although this is not mandatory and a lifting surface approach could be adopted [20][21].

From Green's theorem and previous assumptions, it can be shown that the velocity potential Φ can be written as :

$$\Phi(P,t)=-\frac{1}{4\pi}\iint_{\Sigma}\mu(M)\frac{\vec{r}.\vec{n}_M}{r^3}dS \quad (4)$$

where $\mu(M)=-[\Phi]$ is the opposite of the potential discontinuity at any wake point M, P is any point of the field, $\vec{r}=\vec{MP}$, and $\vec{n}_M$ is the outward normal at M.

This expression shows that the potential Φ is a double-layer potential where μ represents the surface-doublet distribution.

The velocity induced by such a wake at any point in the field is :

$$\vec{grad}\,\Phi(P,t)=\vec{grad}\left(-\frac{1}{4\pi}\iint_{\Sigma}\mu(M)\frac{\vec{r}.\vec{n}_M}{r^3}dS\right) \quad (5)$$

which can be rewritten as :

$$\vec{U}(P,t)=\vec{grad}\,\Phi(P,t)$$
$$=-\frac{1}{4\pi}\iint_{\Sigma}\frac{\left(\vec{n}_M\wedge\vec{\nabla}\mu(M)\right)\wedge\vec{r}}{r^3}dS \quad (6)$$
$$+\frac{1}{4\pi}\int_{\partial\Sigma}\mu(M)\,\vec{grad}\left(\frac{1}{r}\right)\wedge d\vec{M}$$

where $\partial\Sigma$ indicates the oriented edge of Σ, and $\vec{\nabla}\mu$ is the surface gradient defined as :

$$\vec{grad}\,\mu=\frac{\partial\mu}{\partial n}\vec{n}+\vec{\nabla}\mu .$$

Considering the potential continuity between the flowfield and the wake, the doublet's strength μ is equal to zero along the oriented edge $\partial\Sigma$ except at the lifting-line itself [19].

Following the concept of Mudry, the wake S is defined as the location of the material points which constitute the upper surface S^+ and the lower surface S^-. But, since a particle M^+ of S^+ coincident with the particle M^- of S^- at time t has a different velocity $\vec{U}^+(M^+,t)$ from the one of M^- $\vec{U}^-(M^-,t)$, neither physical nor mathematical criteria can favour $\vec{U}^+$ or $\vec{U}^-$ to define the wake velocity $\vec{U}$.

Therefore the median velocity $\vec{U}^*$ proposed by Helmholtz has been chosen to characterise the wake velocity (fig. 2).

$$\vec{U}=\vec{U}^*=\frac{\vec{U}^+ +\vec{U}^-}{2} \qquad (7)$$

Then, the median parametrisation class of a singular surface for $\vec{U}^*$ is introduced, which corresponds to any parametrisation $\vec{\varpi}$ for which

$$\left.\begin{array}{l}(q^1,q^2)\in\Omega\subset IR^2\\ P(x_1,x_2,x_3)\in IR^3\\ t\in I\subset IR\end{array}\right\}\mapsto\vec{OP}=\vec{\varpi}(q^1,q^2,t)\in\Sigma \quad (8)$$

and

$$\forall t\in I\quad\frac{\partial\vec{\varpi}}{\partial t}(q^1,q^2,t)=\vec{U}^*(\vec{\varpi}(q^1,q^2,t),t) \quad (9)$$

where O is the origin of the coordinate system.
Then the wake can be characterised by a non-unique couple ($\vec{\varpi}$, $\vec{\gamma}$), where :

- $\vec{\varpi}$, the median parametrisation, determines the geometrical shape of the vortex sheet and its deformation,
- $\vec{\gamma}$, the associated median vortex density, determines the vortex sheet strength :

$$\vec{\gamma}(q^1,q^2,t)=N\vec{\mu}=\vec{N}\wedge\vec{\nabla}[\Phi]$$
$$=\left(\frac{\partial\vec{\varpi}}{\partial q^1}\wedge\frac{\partial\vec{\varpi}}{\partial q^2}\right)\wedge\vec{\nabla}[\Phi] \quad (10)$$
$$=\gamma^1\frac{\partial\vec{\varpi}}{\partial q^1}+\gamma^2\frac{\partial\vec{\varpi}}{\partial q^2}$$

As the pressure is continuous across the wake, $\vec{\gamma}$ has the fundamental property to conserve its contravariant components γ^1 and γ^2, which can be defined when the particle is released at the trailing edge. This parametrisation allows to represent the sheet in the computational space Ω which does not explicitly depend on time and in which all the integrals of (6) can be solved (fig.3). Moreover, from the γ^1 and γ^2 conservation property, one and only one variable $\vec{\varpi}$ is used. Indeed, the velocity induced by the vortex sheet Σ becomes :

$$\vec{U}(\vec{x},t)=\frac{1}{4\pi}\iint_{\Omega}\frac{\vec{\gamma}(q^1,q^2,t)\wedge\left(\vec{x}-\vec{\varpi}(q^1,q^2,t)\right)}{\left\|\vec{x}-\vec{\varpi}(q^1,q^2,t)\right\|^3}dq^1dq^2$$
$$+\frac{1}{4\pi}\int_{BF}[\phi](q^1,q_0^2,t)\frac{\left(\vec{x}-\vec{\varpi}(q^1,q_0^2,t)\right)\wedge d\vec{\varpi}(q^1,q_0^2,t)}{\left\|\vec{x}-\vec{\varpi}(q^1,q_0^2,t)\right\|^3} \quad (11)$$

with :

$$\vec{\gamma}(q^1,q^2,t)=\gamma^1(q^1,q^2)\frac{\partial\vec{\varpi}}{\partial q^1}(q^1,q^2,t)$$
$$+\gamma^2(q^1,q^2)\frac{\partial\vec{\varpi}}{\partial q^2}(q^1,q^2,t) \quad (12)$$

The particle convection velocity is obtained by adding this induced velocity to the advancing velocity $\vec{V}_e$.

To parametrise the wake, q^1 is chosen as a radial parameter q and the releasing time τ represents the second contravariant variable q^2.

Finally, from a lagrangian representation $\vec{h}(q,t)$ of the trailing edge BF of the blades in the inertial frame :

$$\vec{OP} = \vec{h}(q,t) \qquad (13)$$

the shedding condition of the wake can be defined as $\vec{\varpi}(q,\tau,\tau) = \vec{h}(q,\tau)$ (14).

NUMERICAL IMPLEMENTATION

The numerical procedure consists in dividing the wake surfaces into finite surface elements such that the parametrisation domain Ω is composed of constant subdivision elements (h^1, h^2) (see fig. 3). Hence, the integrals appearing in equation (11) are replaced by finite sums. But contrary to low-order panel methods, the doublet strength μ is not supposed to be constant per panel, but linear, while the surface gradient $\vec{\nabla}[\Phi]$ is constant.

One possible way to define the median vortex density $\vec{\gamma}$ on a quadrilateral doublet panel Ω_j is obtained by applying the Stokes-Ampere law for the potential jump which gives :

$$\begin{aligned}\vec{\gamma} &= \vec{N} \wedge \vec{\nabla}[\Phi] \\ &= \vec{N} \wedge \vec{grad}[\Phi] \qquad (15) \\ &= \int_{\partial\Omega_j} [\Phi] d\vec{l}\end{aligned}$$

This method is applied when the panel is being shed, therefore the contravariant components γ^1 and γ^2 are not yet known. As soon as these components are determined, calculating $\frac{\partial\vec{\varpi}}{\partial q}$ and $\frac{\partial\vec{\varpi}}{\partial\tau}$ vectors is sufficient to characterise the panel.

Induced velocities for a panel are calculated by a numerical Gauss integration method with four points. Using n integration points, the error, in two dimensions, is of $0(\Delta r)^{2n}$ [22]. It must be noticed here that using one integration point only, the method would be equivalent to vortex particle methods. Different wake's representations have been studied :

- vortex particles,
- vortex lattices with $[\Phi]$=cste [18],
- vortex lattices with $\vec{\nabla}[\Phi] = \vec{cste}$ [23],
- triangular panels with Gauss integration,
- quadrilateral panels with Gauss integration.

It was found that the most efficient discretisation in terms of cost-accuracy ratio is the last one which was thus selected for the following work. The computation of bound vorticity on the blade is the result of an iterative process which is described below. Assuming a bound vorticity distribution on the blade, and imposing equation (11) at each quarter-chord point of the blade, allows to estimate the local induced angle of attack. The knowledge of blade motion then allows to compute the total incidence, and consequently the blade loads by using the airfoil tables. The Joukovski theorem, relating local lift to bound circulation, then gives a new estimate of the bound circulation, which may be different from the initial one. Therefore the process has to be repeated until an unique couple $(\Gamma, \vec{U})$ is found.

Once a median vortex density has been assigned to the new row of vortex panels, the wake is moved with the calculated induced velocities plus the velocity components due to the helicopter motion, and the blades are rotated by an angle equal to the azimuthal discretisation step. To start the computation, either an impulsive start from rest can be used or the wake can be initialised by any given geometry and circulation distribution.

The use of a higher order discretisation allows to decrease the degree of singularity of the method from 1/r to log(r). Indeed, it can be shown analytically that the surface integral of (11) converges in the sense of Cauchy's principal value. Consequently, numerical tests have been completed in order to check the behaviour of the numerical integration in the vicinity of a panel surface. Figure 4 shows the results obtained along a diagonal line crossing the panel surface on which a constant doublet intensity was imposed. As can be seen, none of the three velocity components is singular, showing that the integration scheme can work without any regularisation. Therefore, in all the following computations, no regularisation has been applied with the MINT code.

ROTOR BLADE CHARACTERISTIC FEATURES

One particularity of the helicopter rotor is that the wake is shed from several blades so that the sheets trailed from the various blades closely interact between themselves due to the combination of translation and rotation motions. Consequently

the wake deformation process must account for the contribution of all the sheets in order to describe the physical phenomena properly. Furthermore, at each time step, an iterative process is necessary in order to apply the Kutta-Joukovski condition for the various blades and thus shed a vorticity consistent with the lift distribution on the whole rotor. Finally, in the computation, only three blade revolutions are stored in the wake and older panels are not taken into account because their influence is supposed negligible.

Another important topic is related to rotor trim. Indeed, the articulated or soft hub, which is necessary for minimising the periodic hub moments and to control the rotor, introduces a strong coupling between the aerodynamic and the inertial loads, so that the blade motion as well as elastic deformation is the result of a complex aeromechanics problem. In the present computations, the rotor trim was completed externally using the R85/METAR [24] code with a prescribed wake geometry, and the blade kinematics was imposed in the free-wake computation without any additional coupling with the dynamics code.

The combination of rotation and translation motions of the blade also introduces a disymmetry in the advancing velocity of the blade, with high speeds in the advancing blade sector and low speeds for the retreating blade. Therefore transonic conditions are generally encountered in the advancing blade side, so that the incompressible assumption is no more valid. This is why a lifting line approach was chosen, which allows to use 2D airfoil tables to compute the blade loads and thus easily account for first order compressibility effects.

The main drawback of this choice is that 2D airfoil tables do not account for unsteady effects which are constantly present as soon as forward flight is considered. In order to solve this problem, an unsteady lifting line theory [25] is being adapted to the rotor problem for implementation in the free-wake analysis. However, all the results presented in this paper use the steady airfoil tables to compute the blade loads only.

NUMERICAL RESULTS

The testing and validation of the method were done on the BO 105 rotor using the HART database [26]. It concerns a fully instrumented rotor for descent flight conditions and a parametric study of the effect of higher harmonic control on rotor noise and vibration was completed.

Influence of discretisation parameters

In this part, the multicyclic minimum vibration case (MV) for a 6 degrees descent flight with an advance ratio μ=0.15 is considered. This test case showed the occurrence of multiple blade vortex interactions on the advancing blade side.

First, the influence of the azimuthal step $\Delta\Psi$ on the predicted loads is analysed. For this study, a spanwise discretisation of 15 sections was used. The computation was run for the following conditions :

- $\Delta\Psi=10^\circ$ with a prescribed initial wake,
- $\Delta\Psi=10^\circ$ with an impulsive start,
- $\Delta\Psi=5^\circ$ with an impulsive start,
- $\Delta\Psi=2^\circ$ with an impulsive start.

The MINT computation yielded a good convergence for all these azimuthal steps. The figure 5 represents the mean displacement of the wake panels from one revolution to the other. Therefore, it is only plotted when three blade revolutions have been completed for an impulsive start. On the contrary, the initialisation with a METAR wake allows to plot the wake convergence from the first blade revolution. The oscillatory shape of this convergence curve for the METAR wake initialisation is due to the need to transport the wake distortions to the three rotor revolutions considered in the computations. After this has been completed ($\Psi=1080^\circ$), the convergence behaviour of the computation is very similar whatever the initialisation is used. Moreover, the smaller the azimuthal step is, the better the convergence is. However, the computational cost is much larger for small time step discretisation. The computed loads CnM^2 are shown in figure 6 at the section r/R=0.87. As can be seen, more the time step is reduced, more the calculated loads show an oscillatory behaviour between 0° and 90° and between 270° and 310°. These blade sectors correspond to the location of BVI events for this flight condition. However, as long as the time discretisation is larger than the duration of the BVI phenomena, the computed oscillations cannot simulate the actual interactions but are mainly numerical peaks. Thus, significant differences are found between the 5° and 2° cases on the advancing blade side where the typical duration of an interaction is around 3°, while the peaks are very similar on the retreating side where an interaction last for about 5°. Furthermore, the six interactions computed on the advancing blade side with 2° time step are in fairly good agreement with the multiple interactions obtained in the experiment. However, the high resolution 2° computation gives spurious oscillations in the rear part of the rotor disk. This is the place where an accumulation of the wake sheets occurs and since no regularisation is applied, they bring small perturbations to the

solution. Elsewhere, the differences between the various computations are very small, especially between 2° and 5°. Finally, a small phase lag between computation and experiment can be noticed. This may be due either to the quasi-steady assumption of the blade loads or to the blade trim computation.

The influence of spanwise discretisation is now investigated, using an azimuthal step equal to 10° and a spanwise discretisation of :

- 15 sections,
- 30 sections.

Figure 7 shows the load evolution with azimuth at the radial station r/R=0.87. Although some small differences can be found between the two computations, mainly on the amplitude of the CnM^2 evolution, the results are much less dependent on this parameter than on the azimuthal discretisation. This is probably due to the sections distribution along the blade span, which concentrates the control points in the vicinity of the blade tip where the main aerodynamic phenomena occur. This is confirmed by figure 8, where the spanwise load evolution is plotted for the azimuth Ψ=120° (where the interacting vortices are generated). Indeed, the two computations give very similar results, and therefore a spanwise discretisation of 15 sections has been selected.

Influence of the initialisation

It is important to check that the convergence of the time marching algorithm is independent of the initial condition for steady flight conditions. Therefore the same computation was completed using either an impulsive start or a prescribed helical wake geometry plus a given circulation distribution obtained from a R85/METAR computation. The same test case as above was considered (BO 105 rotor, MV case) and the following discretisation was used :

- $\Delta\Psi$=10°,
- 15 spanwise stations.

Figure 9 shows a comparison of the computed loads after convergence. For both computations, 5 blade revolutions were computed. The computed loads are almost identical, which shows that the results are independent on the initial conditions, for a steady flight condition. However, the use of a prescribed wake initialisation is less efficient for the following reasons :

- it is necessary to convect this initial wake out of the range considered in the computation in order to reach convergence,
- a large number of wake panels has to be considered as soon as the calculation is started.

COMPARISON WITH MESIR

In this paragraph, the MINT predicted loads are compared with experiment and with MESIR computations. Two test configurations for BO 105 rotor have been selected from the HART tests. They are the baseline case (BA), and the minimum vibration case (MV) for a 6 degrees descent flight and an advance ratio of 0.15.

Figure 10 shows the loads evolution with azimuth for the MV case at the radial station r/R=0.87. The same comparison is shown for the BA case in figure 11. Exactly the same discretisation in azimuth and span is used for MESIR and MINT. Generally, the MINT computation provides a smoother solution than MESIR, where oscillations are found on the rear part of the rotor disk. This is probably due to the higher order of discretisation of MINT which reduces the order of singularity of the vortex sheet compared to MESIR. This is particularly noticeable because no numerical regularisation is applied in MINT while a regularisation has to be used in MESIR. The smoother evolution of the MINT results compared to the MESIR results is confirmed in figures 12 and 13, which show a close view of the sheet shed from one blade for the BA case.

Another interesting feature of MINT is that it allows to reduce the computing cost significantly (fig. 14). For an impulsive start and a standard discretisation (20 radial stations and 36 time steps per revolution) the computing cost is divided by a factor of three.

CONCLUSIONS AND PERSPECTIVES

A new time-marching panel method has been developed to compute helicopter rotor wakes. It is based on a general mathematical theory of the evolution of vortex-sheets in an inviscid, incompressible, unsteady flow. The numerical implementation was made with the lifting-line assumption to simulate the rotor blades. High order panels and a numerical integration technique have been used ; it was found that no numerical regularisation is necessary to avoid a singular behaviour in the vicinity of the wake. The validation on a helicopter in steady forward flight showed that

the method is very robust. Converge of the method can be achieved even for azimuthal steps of the order of BVI phenomena which are thus captured. It was checked that the converged solution is independent on the initialisation. In addition, this new method allows a significant computing time reduction compared to the MESIR code currently used at ONERA.

In order to be able to deal with general flight conditions such as manoeuvre, an unsteady lifting-line approach is being developed to provide a better description of the blade aerodynamics.

ACKNOWLEDGEMENT

The authors are very grateful to Michel Mudry who is the supervisor of Gaëlle Coppens's doctoral thesis.

REFERENCES

1. Schmitz, F.H., and Yu, Y.H., « Helicopter Impulsive Noise : Theoretical and Experimental Status », Journal of Sound and Vibration, 109 (3), pp 361-422, 1986.
2. Landgrebe, A.J., « New Directions in Rotorcraft Computational Aerodynamics Research in the U.S. », AGARD Conference Proceedings No. 552, Aerodynamics and Aeroacoustics of Rotorcraft, 75th Fluid Dynamics Symposium, Berlin, Germany, October 10-13, 1994.
3. Dacles-Mariani, J., Rogers, S., Kwak, D., Zilliac, G., and Chow, J., « A Computational Study of Wingtip Vortex Flowfield », AIAA Paper 93-3010, 24th Fluid Dynamics Conference, Orlando, FL, July 6-9, 1993.
4. Raddatz, J, and Pahlke, K, « 3D Euler Calculations of Multibladed Rotors in Hover : Investigation of the Wake Capturing Properties », AGARD Conference Proceedings No. 552, Aerodynamics and Aeroacoustics of Rotorcraft, 75th Fluid Dynamics Symposium, Berlin, Germany, 10-13 october 1994.
5. Rouzaud, O., Raddatz, J., and Boniface, J.C., « Euler Calculations of Multibladed Rotors in Hover and Comparison with Helishape Tests », American Helicopter Society 53rd Annual Forum Proceedings, Virginia Beach, VA, April 29-May 1, 1997.
6. Felici, H.M., and Drela, M., « Reduction of Numerical Diffusion in Three-Dimensional Vortical Flows Using a Coupled Eulerian/Lagrangian Solution Procedure », AIAA Paper 93-2928, 24th Fluid Dynamics Conference, Orlando, FL, July 6-9, 1993.
7. Nastasi, V., « Etude Numérique du Tourbillon d'Extrémité de Pale du Rotor d'Hélicoptère en Régime Compressible », Ph. D. Thesis, Paris VI University, France, October 1997.
8. Steinhoff, J., and Raviprakash, G.K., « Navier-Stokes Computation of Blade-Vortex Interaction Using Vorticity Confinement », AIAA Paper 95-0161, 33rd Aerospace Sciences Meeting and Exhibit, Reno, NV, January 9-12, 1995.
9. Steinhoff, J., and Ramachandran, K., « A Vortex Embedding Method for Free-Wake Analysis of Helicopter Rotor Blades in Hover », 13th European Rotorcraft Forum, Arles, France, September , 1987.
10. Bridgeman, J.O., Ramachandran, K., Caradonna, F.X., and Prichard, D., « A Computational Analysis of Parallel Blade-Vortex Interactions Using Vorticity Embedding », American Helicopter Society 50th Annual Forum Proceedings, Washington D.C., USA, May 11-13, 1994.
11. Visingardi, A., D'Alascio, A., Pagano, A., and Renzoni, P., « Validation of CIRA's Rotorcraft Aerodynamic Modelling System with DNW Experimental Data », 22nd European Rotorcraft Forum, Brighton, U.K. Spetember 17-19, 1996.
12. Lee, D.J., and Na, S.U., « Predictions of Airloads and Wake Geometry for Slowly Starting Rotor Blades in Hovering Flight by Using Time Marching Free Vortex Blob Method », American Helicopter Society 52nd Annual Forum Proceedings, Washington D.C., June 4-6, 1996.
13. Cantaloube, B, and Huberson, S., « Calcul d'écoulements de fluide incompressible non-visqueux autour de voilures tournantes par une méthode de singularités », La Recherche Aérospatiale, n°6, pp.403-415, 1984.
14. Schaffar, M., Hearth, J., and Gnemmi, P., « Computation of the BVI noise for the BO105 Model Rotor in Forward Flight and Comparison with Wind Tunnel Tests », American Helicopter Society 47th Annual Forum Proceedings, Phoenix, AZ, May 6-8, 1991.
15. Wachspress, D.A., and Quackenbush, T.R., « Wake Model Requirements for Prediction of BVI Airloads », American Helicopter Society Technical Specialists'Meeting for Rotorcraft Acoustics and Aerodynamics, Williamsburg, VA, October 28-30, 1997.
16. Bagai, A., and Leishman, J.G., « Rotor Free-Wake Modeling using a Relaxation Technique Including Comparisons with Experimental Data », American Helicopter Society 50th

Annual Forum Proceedings, Washington D.C., May 11-13, 1994.
17. Ahmed, S.R., « Prediction of Blade Vortex Interaction Aerodynamics for a Higher Harmonic Controlled Rotor », AIAA Paper 96-1698, 2nd AIAA/CEAS Aeroacoustics Conference, State College, PA, May 6-8, 1996.
18. Michéa, B., Desopper, A., and Costes, M., « Aerodynamic Rotor Loads Prediction Method with Free Wake for Low Speed Descent Flights », 18th European Rotorcraft Forum, Avignon, France, September 15-18, 1992.
19. Mudry, M., « La théorie générale des nappes tourbillonnaires et ses applications à l'aérodynamique instationnaire », Ph. D. Thesis, Paris VI University, France, July 1982.
20. Leroy, A., « Une méthode générale de calcul des systèmes portants et/ou propulsifs minces (fluide parfait incompressible en écoulement instationnaire) », Ph. D. Thesis, Orléans University, France, March 1997.
21. Leroy, A. and Devinant, P., « A general Approach for Computing unsteady 3D thin Lifting and/or Propulsive Systems derived from a Complete Theory », International Journal for Numerical Methods in Fluids, to be published.
22. Imbert, J.F., « Analyse des structures par éléments finis », Cepadues éditions, Sup'Aero.
23. Cantaloube, B. and Rehbach, C., « Calculation of the Integrals of the Singularities Methods », La Recherche Aérospatiale, 1986.
24. Arnaud, G. and Beaumier, P., « Validation of R85/METAR on the Puma RAE Flight Tests », 18th European Rotorcraft Forum, Avignon, September 15-18, 1994.
25. Devinant, P., « An Approach for unsteady Lifting-Line Time-Marching Numerical Computation », International journal for Numerical Methods in Fluids, vol. 26, pp.177-197, 1998.
26. Kube, R. and al., « HHC Aeroacoustic Rotor Tests in the German Dutch Wind Tunnel : Improving Physical Understanding and Prediction Codes », American Helicopter Society 52nd Annual Forum Proceedings, Washington D.C., June 4-6, 1996.

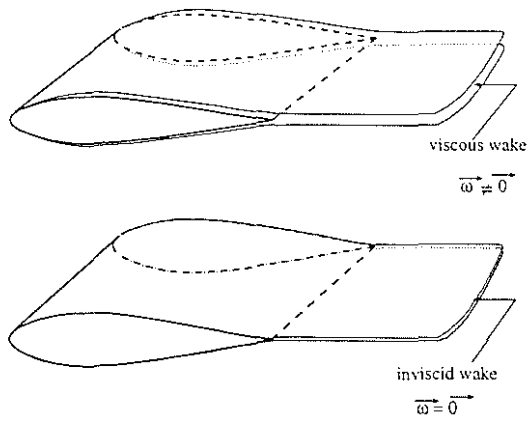

fig. 1 Illustration of shedding wakes.

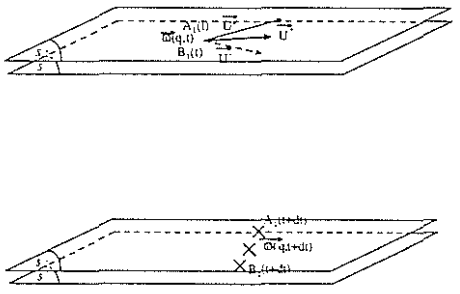

fig. 2 Median plane notion.

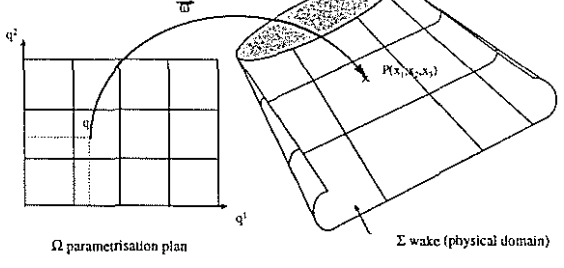

fig. 3 Correspondence between vortex-sheet and parametrisation

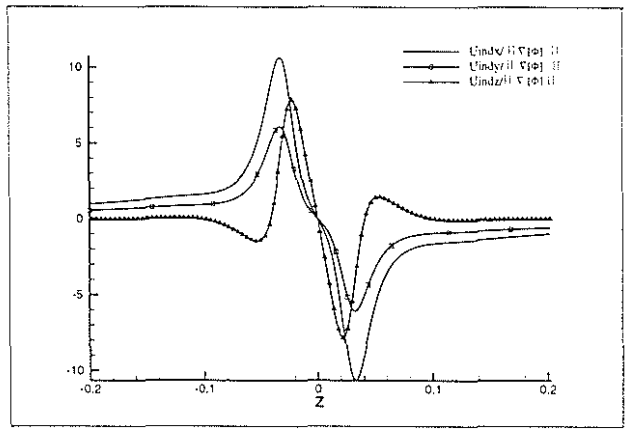

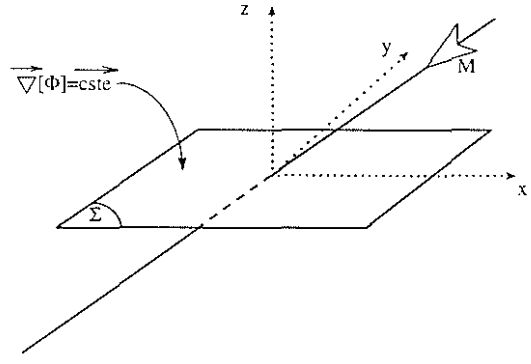

fig. 4 Analysis of velocity behaviour in the vicinity of the wake.

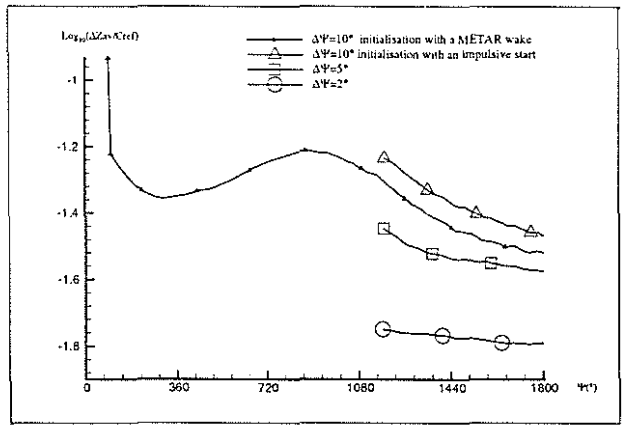

fig. 5 Free wake convergence. MV.

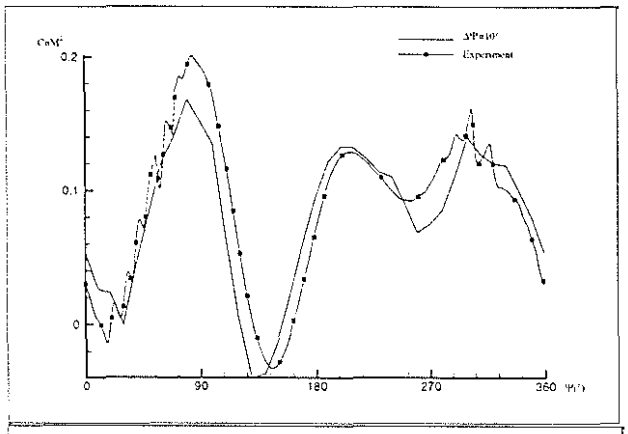

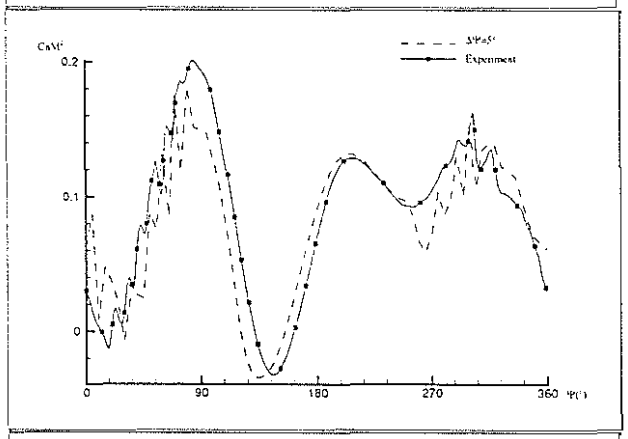

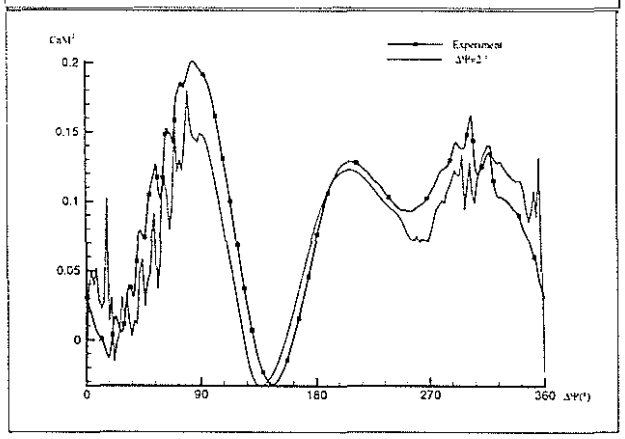

fig. 6 Effect of azimuthal discretisation at r/R=0.87 for the Minimum Vibration case.

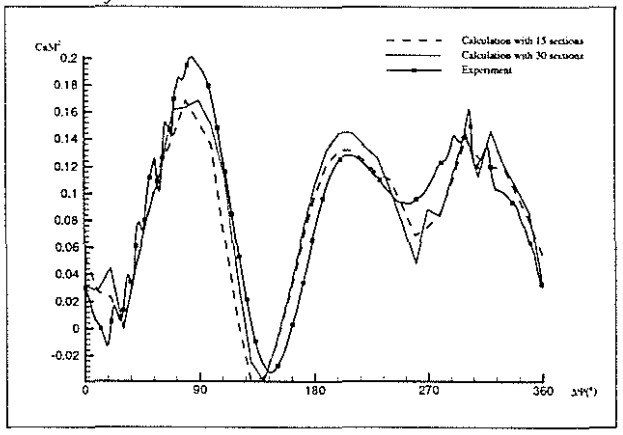

fig. 7 Effect of spanwise discretisation at r/R=0.87. MV

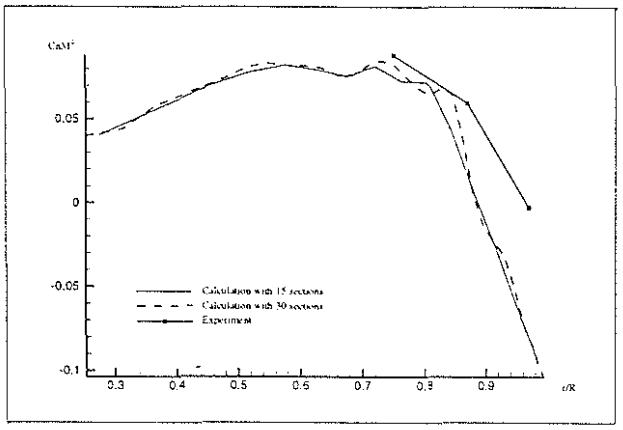

fig. 8 Effect of spanwise discretisation at Ψ=120°. MV.

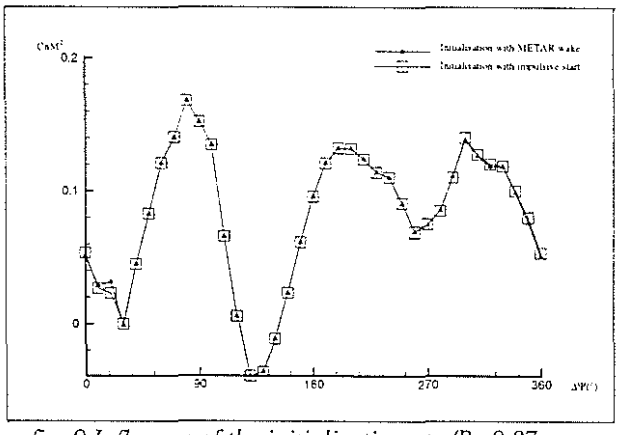

fig. 9 Influence of the initialisation at r/R=0.87. MV.

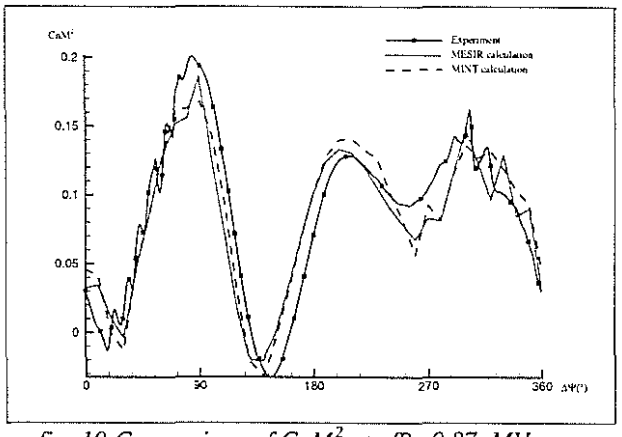

fig. 10 Comparison of CnM^2 at r/R=0.87. MV.

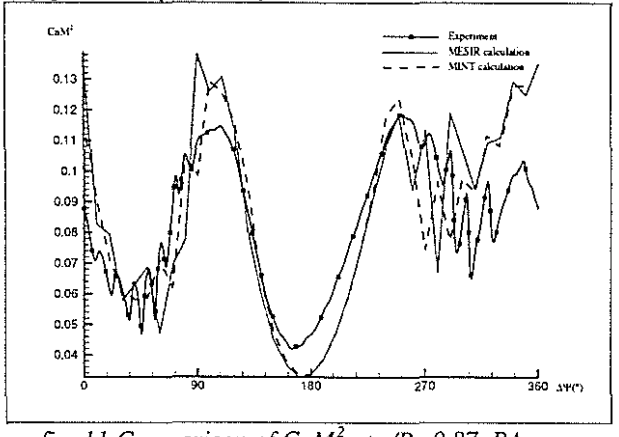

fig. 11 Comparison of CnM^2 at r/R=0.87. BA.

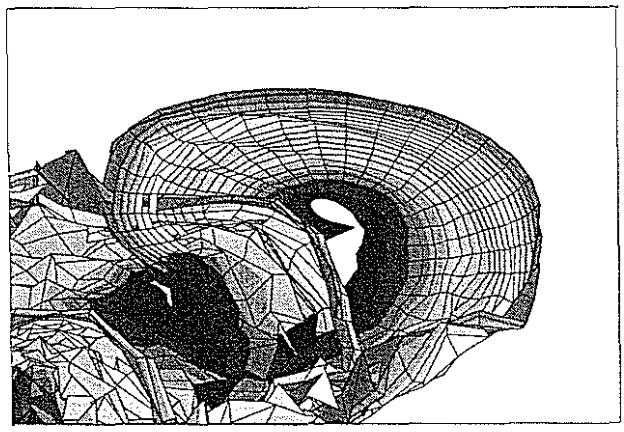

fig. 12 MESIR wake geometry.BA.

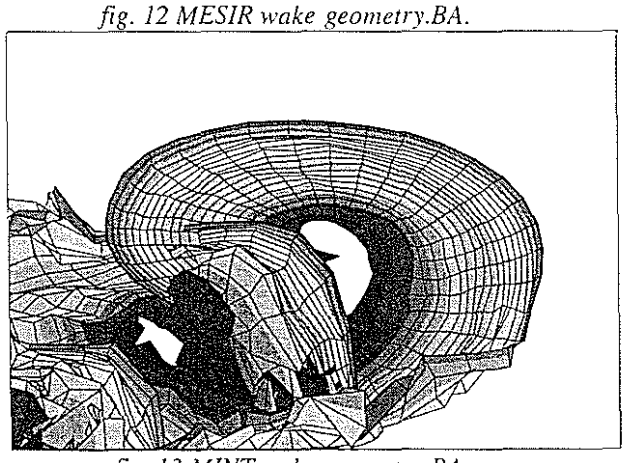

fig. 13 MINT wake geometry.BA.

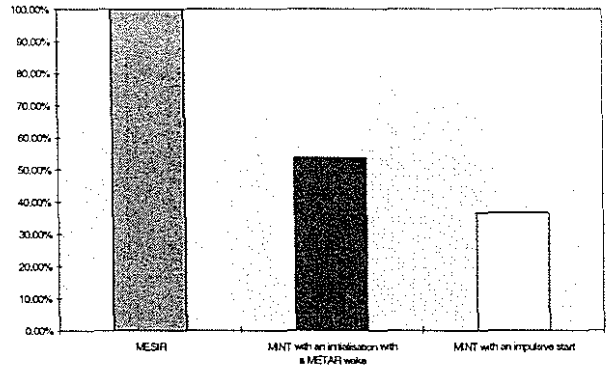

fig 14 Comparison of CPU time. MV.